Encapsulation of Poly(3-hexylthiophene) J-Aggregate Nanofibers with an Amphiphilic Block Copolymer

ARTICLE *in* LANGMUIR · OCTOBER 2012

Impact Factor: 4.46 · DOI: 10.1021/la3034337 · Source: PubMed

4 AUTHORS, INCLUDING:

Jian Gao
Lawrence Berkeley National Laboratory
16 PUBLICATIONS **102** CITATIONS
SEE PROFILE

Amanda Kamps
University of Pennsylvania
10 PUBLICATIONS **133** CITATIONS
SEE PROFILE

John K Grey
University of New Mexico
26 PUBLICATIONS **397** CITATIONS
SEE PROFILE

Langmuir

Article

pubs.acs.org/Langmuir

Encapsulation of Poly(3-hexylthiophene) J-Aggregate Nanofibers with an Amphiphilic Block Copolymer

Jian Gao,[†] Amanda Kamps,[‡] So-Jung Park,[‡] and John K. Grey*[,†]

[†]Department of Chemistry and Chemical Biology, University of New Mexico, Albuquerque, New Mexico 87131, United States

[‡]Department of Chemistry, University of Pennsylvania, Philadelphia, Pennsylvania 19104, United States

Supporting Information

ABSTRACT: Poly(3-hexylthiophene) (P3HT) nanofibers (NF) displaying J-aggregate exciton coupling behavior are encapsulated with the amphiphilic block copolymer (BCP), poly(3-hexyl-thiophene)-block-poly(ethylene-glycol), (PHT_{20}-b-PEG_{108}). Encapsulation results in the formation of hierarchical superstructures, and the BCP coating is expected to exert a mild chemical pressure on the periphery of the NFs. Photoluminescence from encapsulated NF superstructures show line shape distortions due to self-absorption of the 0−0 transition which is consistent with preservation of J-aggregate character (intrachain order). Detailed resonance Raman spectra of encapsulated BCP-NF structures show no discernible changes in the P3HT aggregation state, and overtone and combination bands involving the symmetric stretching C═C (∼1450 cm^{-1}) and C−C (∼1380 cm^{-1}) backbone modes are observed. These features permit quantitative estimates of vibrational mode-specific excited state structural displacements using a time-dependent Raman intensity analysis which is not possible from conventional vibronic analysis of optical lineshapes.

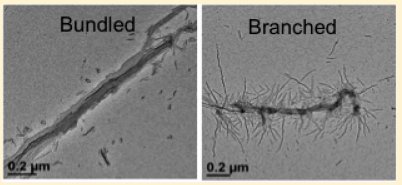

INTRODUCTION

Understanding the delicate interplay between intrachain order and interchain exciton coupling in π-stacked conjugated polymer aggregates is crucial for optimizing their performance in devices such as solar cells.[1−5] This relationship manifests in aggregates of the conjugated polymer, poly(3-hexylthiophene) (P3HT), where subtle changes in chain conformation and packing can translate into large changes in exciton coupling characteristics.[6] Because aggregates promote efficient charge and energy (exciton) transport,[7−11] it is advantageous to understand the specific structural factors regulating electronic coupling in the close-packed chains comprising the aggregate. However, this is complicated in thin films due to the stochastic nature of solution processing techniques (i.e., spin-coating) and polydispersity effects resulting in randomly oriented aggregates, varying sizes, and lower crystallinity and aspect ratios.

Solution-based self-assembly techniques have recently emerged as a promising strategy for effectively managing the order−disorder boundaries in P3HT aggregates by fractionating molecular weights.[12−16] Fractionation effectively lowers the polydispersity index and allows aggregates to grow into nanofibers (NFs) with large aspect ratios and a smaller amount of stacking faults. Furthermore, this approach permits fine-tuning of chain conformation and order which determine exciton coupling characteristics of P3HT aggregates. Spano and co-workers demonstrated that optical spectra of P3HT aggregates can be used to infer correlations between chain conformation (intrachain order or planarity of monomers) and packing characteristics on the type and strength of exciton coupling.[17,18] For example, comparison of 0−0 and 0−1 vibronic ratios provides a facile means to estimate the type and strength of exciton coupling where 0−0/0−1 < 1 and 0−0/0−1 > 1 indicate H- and J-aggregation, respectively.[17] The appearance of either aggregate type is determined primarily by intrachain order where low intrachain order results in increased interchain coupling and optical spectra resemble H-aggregates. Conversely, high intrachain order favors larger intrachain coupling and lower interchain coupling, and spectra resemble J-aggregates.[17,19,20] Deposition of P3HT thin films by solution spin-casting techniques does not promote molecular weight fractionation and, consequently, aggregate optical lineshapes appear predominantly H-like.[21,22] J-aggregate character is much more elusive in P3HT aggregates and usually only appears in samples with low polydispersity, high regioregularity (>95%) and, most importantly, high intrachain order.[23] P3HT NFs self-assembled in toluene show pronounced J-aggregate character (i.e., 0−0/0−1 >1) originating from highly elongated P3HT chains with high intrachain order.[24] Temperature- and pressure-dependent spectroscopy studies of J-type NFs also demonstrated a high sensitivity of intrachain order to minor structural perturbations of the NF packing. For example, Niles et al. applied external pressures of up to ∼20 kbar on NFs dispersed in solid solutions and pressure-dependent photoluminescence (PL) spectra showed a distinct change from J- to H-aggregate behavior. This effect was suggested to arise from a repacking of P3HT alkyl side groups from a type I to a type II arrangement, which causes the observed transition from J- to H-type behavior. Baghgar et al. also demonstrated that single P3HT NFs assembled in anisole can exhibit both H- and J-type emission suggesting multiple

Received: August 26, 2012
Revised: October 24, 2012
Published: October 30, 2012

domains.[25] We now further investigate the influence of minor structural perturbations on the sensitive relationship between intrachain order and exciton coupling characteristics by encapsulating J-type P3HT NF aggregates using an amphiphilic block copolymer (BCP), poly(3-hexyl-thiophene)-block-poly-(ethylene-glycol), (PHT_{20}-b-PEG_{108}).

Kamps et al. recently used this BCP system to encapsulate H-type NFs of P3HT prepared from anisole solutions.[26] Unlike NFs assembled in toluene, anisole is a poor solvent and molecular weight fractionation is minimal. Intrachain order in these aggregates is correspondingly low, hence, the appearance of predominantly H-type character. Upon encapsulation by the BCP system, NFs retained H-aggregate character suggesting interactions between the NF and BCP molecules are minor and do not appreciably affect interchain exciton coupling.[26] Furthermore, it was demonstrated the encapsulated NFs assemble into secondary superstructures and take on branched and bundled morphologies depending on the choice of surrounding medium. Compared to variable pressure techniques, encapsulation of J-type NFs by BCP molecules represents a milder structural perturbation and thus provide an excellent means to explore the extent to which intrachain order can be tuned.

A key goal of this work is to ascertain whether interactions between the NF and BCP coating alter chain packing, intrachain order and, hence, exciton coupling in J-type NFs using optical spectroscopy and single particle PL spectroscopy. Additionally, resonance Raman spectroscopy is performed on encapsulated NF superstructures to uncover changes to the structural integrity of the aggregate. Raman spectra reveal detailed overtone and combination transitions rarely observed in conjugated polymers that expose valuable insights into excited state geometry changes normally masked in optical spectra of P3HT aggregates. For example, nonzero exciton coupling leads to distortions of the optical lineshapes (i.e., attenuated or enhanced 0−0 transitions in H- or J-type couplings, respectively).[17] A time-dependent analysis of Raman intensities (fundamentals and overtones) is used to generate estimates of vibrational mode-specific excited state geometrical displacements (Huang−Rhys factors) independent of exciton coupling effects. This approach yields a more complete picture of the multimode excited state structural deformations of aggregated P3HT chains masked in conventional optical spectra.

EXPERIMENTAL SECTION

P3HT NF and the BCP molecules were prepared and characterized according to procedures described in the literature.[5,13,24,26,27] In a typical encapsulation experiment with a molar ratio of BCP:P3HT of 173:1, 800 μL of a 5×10^{-5} M stock solution of BCP in chloroform (concentration determined from UV−vis with an extinction coefficient of 4×10^4 M^{-1} cm^{-1}) was first dried under nitrogen. Then, a 10 μL aliquot of a $\sim 10^{-5}$ M stock solution of P3HT NFs in toluene (concentration estimated from UV−vis assuming an extinction coefficient of 1×10^4 M^{-1} cm^{-1} per monomer) was added to the dried BCP. After 20 min of mixing, either 1000 μL of water or 1000 μL of methanol were added to the solution. The assemblies were mixed for 15 h, and low flow of nitrogen was used to evolve residual toluene in the solution. After dissipation of any residual toluene, either methanol or water was added to the solution until a final volume of 1 mL of solution was reached. In some cases, the superstructures were purified and concentrated by centrifugation at 1000 rpm for 45 min. The NFs were characterized by transmission electron microscopy (TEM) imaging where the samples were prepared by placing a droplet of the NF solution on TEM grids. Solution dispersions of encapsulated NF structures were also investigated using optical absorption and photoluminescence spectroscopy. Samples were then drop-casted on clean glass coverslips for confocal spectroscopy and imaging. Resonance Raman spectra of encapsulated NF structures were measured using a confocal imaging spectrometer described in detail previously.[28]

RESULTS AND DISCUSSION

We first begin by comparing nanoscale structural features of P3HT NF displaying H- and J-aggregate signatures in optical spectra that will later prove useful for correlating changes in exciton coupling upon encapsulation by the BCP system. Figure 1a shows a TEM image of NFs prepared from anisole,

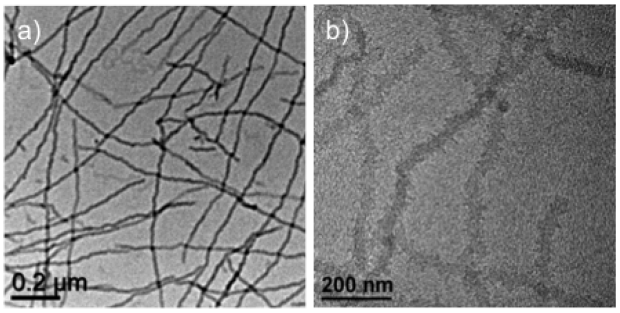

Figure 1. TEM images of pristine (a) H- and (b) J-aggregate NFs. H- and J-type NFs were prepared from anisole and toluene with average widths of ∼20 nm and ∼40 nm, respectively.

and Figure 1b shows those assembled from toluene. The former consisted of P3HT chains with ∼200 monomers whereas those assembled in toluene were fabricated from molecules with ∼350 monomers; however, this difference in molecular weight has little impact on the type of aggregate formed. NFs formed in anisole are narrower (∼20 nm widths) and have larger aspect ratios whereas those formed in toluene are considerably wider (∼40 nm widths) with smaller aspect ratios. From previous work, the former possess H-aggregate character with substantially smaller 0−0/0−1 ratios in absorption spectra, and the latter exhibit pronounced J-aggregate character.[12,27] These results support the previously proposed structural attributes leading to J-type behavior in these NF aggregates whereby P3HT chains are much more elongated than in H-aggregates thus favoring increased intrachain order.[24,29]

Figure 2 shows representative TEM images of encapsulated J-aggregate P3HT NF structures dispersed in methanol and water and cast onto TEM grids. Similar to previous work, two distinct types of secondary structures are observed, namely, branched and bundled.[26] Bundled assemblies of encapsulated NF are mostly observed for samples dispersed in methanol whereas branched structures are obtained for those dispersed in water. However, comparison of the structures shown in Figure 2 to those obtained by Kamps et al. for H-aggregate type NFs show smaller aspect ratios which may arise from instability of the J-aggregate structure in the NF growth direction (i.e., in the direction of the π-stack). To test this hypothesis, solution dispersions of J-type NFs were subjected to sonication treatments that resulted in smaller aspect ratios (see Supporting Information) but retained J-aggregate character. Similar findings were obtained by Niles et al., namely, aspect ratios of J-aggregate NFs decrease upon dilution into inert host matrices, but J-type behavior is preserved. Although TEM studies are helpful for understanding basic packing character-

dx.doi.org/10.1021/la3034337 | Langmuir 2012, 28, 16401−16407

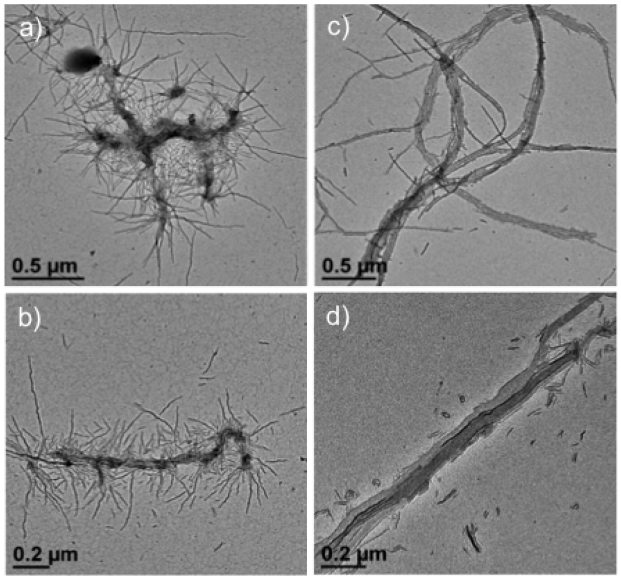

Figure 2. TEM images of branched (a, b) and bundled (c, d) encapsulated P3HT NF superstructures.

istics of NFs within the secondary superstructures, they cannot reveal how intrachain order and interchain coupling are affected by encapsulation.

Optical absorption and PL spectroscopy are used to estimate exciton coupling characteristics of encapsulated NFs through the partially resolved vibronic transitions. Figure 3a shows

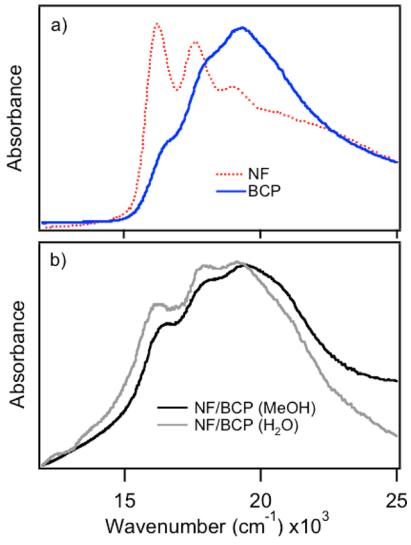

Figure 3. (a) Absorption spectra of pristine P3HT NF (red dotted trace) in toluene and BCP in methanol (blue solid trace). (b) Absorption spectra of encapsulated NF dispersed in methanol (black) and water (gray).

optical absorption spectra of pristine P3HT NF J-aggregates (red dotted trace) and aggregates of the amphiphilic BCP (blue solid trace). The absorption lineshapes of the NFs appear identical to those published previously and those of the BCP resemble H-aggregates.[24−26] Figure 3b shows absorption spectra upon encapsulation for both water and methanol dispersions. Lineshapes display predominant H-type tentatively indicating intrachain order is lower in the encapsulated NFs. Spectral linewidths also become larger in encapsulated samples suggesting increasing inhomogeneity. Despite distinctly different absorption lineshapes of encapsulated NFs from their pristine spectra, it is difficult to quantify the change in exciton coupling since BCP molecules also aggregate when coating the NFs. Absorption vibronic intensity ratios, therefore, are not reliable for determining changes in exciton coupling strength in the encapsulated NFs. Ensemble solution phase PL measurements were performed on both types of encapsulated superstructures but yields are very small making it difficult to obtain reliable estimates. This result suggests that NF emission is probably quenched by efficient excitation energy transfer to the BCP coating which exhibits weak PL signals (see Supporting Information).

We overcome the issue of weak PL yields of encapsulated NFs by using confocal PL imaging capable of single photon detection with far greater sensitivity than ensemble PL measurements. Figure 4 shows representative PL spectra and

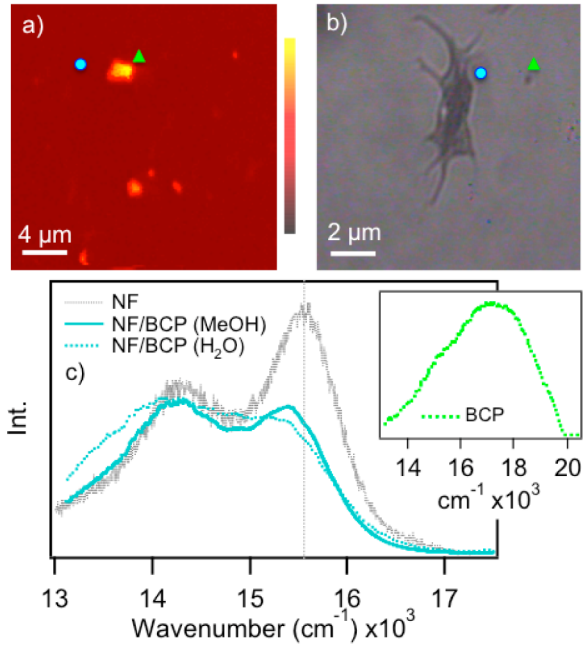

Figure 4. (a) PL and (b) optical images of encapsulated NF samples. Green triangles and blue circles denote amorphous BCP agglomerates and NF superstructures, respectively. (c) Ensemble averaged PL spectra of branched (dotted blue trace) and bundled (solid blue trace) NF superstructures. A representative PL spectrum of pristine NFs is shown for comparison (black dotted trace). Inset: PL spectrum of amorphous BCP particles.

images from both branched and bundled encapsulated NF superstructures generated with 488 nm excitation. PL and optical images are displayed in Figure 4a,b demonstrating evidence for both diffraction-limited and larger (>1 μm) particle sizes. PL spectra of bright spots show higher energy and broad lineshapes resembling amorphous (disordered) P3HT chains (Figure 4c inset). Since these types of lineshapes do not appear in solution phase ensemble PL spectra, we suspect that BCP molecules agglomerate during spin-casting which is reasonable due to the large excess used in the encapsulation process. Corresponding optical images demonstrate that weaker PL spots correspond to the encapsulated NFs that appear to agglomerate when cast on bare substrates. Representative PL spectra of these individual superstructures are shown in Figure 4c for branched (blue dotted) and bundled

dx.doi.org/10.1021/la3034337 | Langmuir 2012, 28, 16401−16407

(blue solid) structures. Compared to pristine J-aggregate NF lineshapes, encapsulated NFs from both dispersions appear H-like where the 0−0 intensity is slightly smaller than the 0−1 sideband. We estimate that PL yields are ∼10−20% of that of pristine NFs from comparison of PL images generated under the same excitation conditions. This unexpected reduction in J-type NF PL intensity confirms efficient energy transfer to nonemissive traps probably on the BCP coating.

On the basis of absorption lineshapes of encapsulated NFs, it is tempting to infer a change from J- to H-aggregate behavior which would suggest that indeed encapsulation induces a small perturbation of NF intrachain order. However, closer inspection of the encapsulated NF PL lineshapes reveals discrepancies in the vibronic intervals, namely, a nonconstant progression frequency across the line shape. This effect is most apparent when comparing lineshapes between pristine and encapsulated NFs where the 0−0 maximum of the latter appears ∼100−200 cm^{-1} lower in energy. The low energy regions of both branched and bundled NF superstructures, on the other hand, overlap well with the pristine NF PL lineshapes. We attribute the discrepancy of the 0−0 transition to self-absorption effects that are especially problematic for J-aggregate emitters due to their smaller Stokes shifts and normally higher PL yields. The chief reason for enhanced self-absorption in encapsulated NFs is their close proximity (see Figure 2) leading to effective high local concentrations. Similar effects were also reported in recent spectroscopic and scanned probe imaging studies of oligothiophene aggregates that show a range of both H- and J-type PL lineshapes.[30] PL line shape distortions from self-absorption occurs in ∼80% of all particles studied, making it difficult to reliably estimate changes in exciton coupling using the PL 0−0/0−1 vibronic peak intensity ratios. Additionally, the appearance of an amorphous PL component in images and spectra (Figure 4a) may indicate a loss of NF structural integrity (aggregated P3HT chains) or excess BCP. To better understand possible changes in the NF structure upon encapsulation, we use resonance Raman spectroscopy which is highly sensitive to local (molecular-level) structure and packing of P3HT chains.

Previously, Gao et al. demonstrated the usefulness of resonance Raman spectra to discern the relative amounts of aggregated (i.e., well-ordered π-stacked chains) and amorphous (i.e., disordered or solution-like) chains in P3HT systems.[28] Namely, Raman bands of the C═C symmetric stretching mode of the P3HT backbone show contributions from both aggregated and amorphous chains with characteristic frequencies of ∼1450 cm^{-1} and ∼1470 cm^{-1}, respectively. Because of the linear relationship between Raman intensity and concentration of scatterers, the relative integrated intensities of both species reveals their relative amounts in the sample. Despite the inconclusive nature of changes in exciton coupling from both absorption and PL spectra, the significant loss of PL intensity in encapsulated NFs permits the measurement of resonance Raman spectra without large PL background interference normally encountered in P3HT J-aggregates.[24] If the amorphous PL signal observed in confocal imaging originates from increased amorphous regions in NF structures or partial dissociation then it should be apparent in resonance Raman spectra, i.e., lower relative intensity from the aggregated contribution and increase in the amorphous component. Figure 5a shows a representative Raman spectrum from an encapsulated NF superstructure and spectra from either branched or bundled structures yielded similar patterns. This

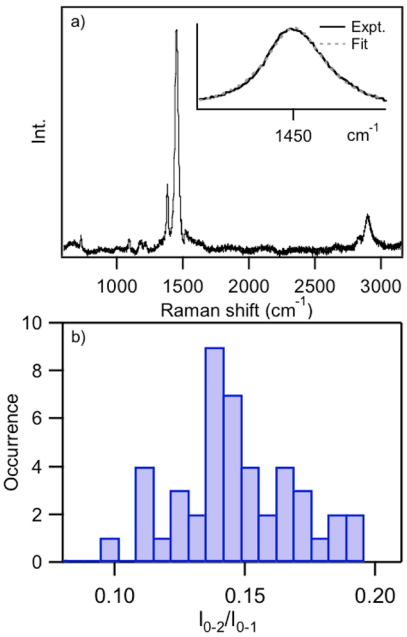

Figure 5. (a) Resonance Raman spectrum of encapsulated NF superstructures showing the first overtone region. Inset: C═C stretching band of P3HT with Lorentzian fit. (b) Histogram of first overtone (0−2) and fundamental (0−1) intensities of the C═C mode.

result is expected since Raman is not capable of discerning exciton coupling but, rather, only changes in polarizabilities of chemical bonds due to changes in local environments (i.e., aggregation) of P3HT chains. Inspection of the dominant C═C lineshapes shows no evidence for an amorphous contribution at ∼1470 cm^{-1} and can be reproduced well with a single Lorentzian function indicating only aggregated P3HT chains from NF. We conclude that contributions from amorphous P3HT in PL images and spectra originates from free BCP molecules not participating in the encapsulation of NFs. Moreover, the Raman scattering cross sections of the BCP molecules are significantly smaller than P3HT at the excitation wavelength used (488 nm) which eliminates the possibility of substantial cross-talk in the measured Raman intensities (see Supporting Information).

Perhaps the most noteworthy aspect of Raman spectra is the appearance of overtones and combination bands of the dominant C═C mode in the high frequency region. These features are rarely reported in conjugated polymers of this class and reveal important insights into the excited state geometries of aggregated P3HT chains. More importantly, Raman spectra are not susceptible to line shape distortion effects encountered in steady-state PL and absorption spectra due to exciton coupling effects and energy transfer. From Figure 5a, the first overtone of the C═C mode appears at ∼2900 cm^{-1} and a combination band corresponding to one quantum of the C═C and C−C (∼1380 cm^{-1}) modes at ∼2840 cm^{-1} lower in intensity. Fundamentals of thiophene ring C−H stretches are also expected in this region (∼2900−3000 cm^{-1}) but their activities are expected to be small since they do have significant displacements in the excited state (i.e., not resonantly enhanced). Indeed, comparison of resonance Raman spectra in Figure 5 with IR and off-resonance Raman spectra of encapsulated NFs showed no overlap or similarity in intensity

dx.doi.org/10.1021/la3034337 | Langmuir 2012, 28, 16401−16407

patterns as the overtone−combination bands in Figure 5a (see Supporting Information).

Because nonzero exciton coupling in aggregate structures results in non-Poissonian optical lineshapes, it is often difficult to determine how much vibrational displacements are affected by electronic delocalization within the π-stacks, i.e., exciton bandwidths.[17] It is typically assumed that these displacements do not change significantly from ideal values determined from single oligothiophenes which can be been difficult to corroborate from optical absorption and PL spectra of P3HT aggregates.[17] Moreover, the low resolution of vibronic structure in optical spectra conceals contributions from other displaced modes, and only the high frequency C=C mode is included in line shape analysis procedures which can lead to overestimation of its actual displacement. To first gain a qualitative understanding of how much overtone features change between superstructures, we estimate the ratio of overtone (0−2) and fundamental intensities (0−1) of the dominant C=C Raman band which is related to its displacement.[31,32] Figure 5b shows a histogram of the 0−2/0−1 integrated intensity ratios for the dominant C=C stretch from individual encapsulated NF superstructures. The 0−2/0−1 values change by almost a factor of 2, indicating excited state geometrical deformations are sensitive to variations in local environments. However, there was also no appreciable difference in 0−2/0−1 values between branched and bundled structures demonstrating insensitivity to longer range interactions between neighboring NFs and the BCP coating.

Raman intensities in Figure 5 can now be analyzed to quantitatively estimate mode-specific vibrational displacements with the aid of the overtone−combination bands. We use the time-dependent theory of Raman spectroscopy developed by Heller, Zink, and co-workers to calculate Raman intensities in Figure 5a.[31−33] Only modes with nonzero displacements contribute to the resonance Raman spectrum, and the relative intensities reveal the slope or horizontal displacement of the potential minima between the ground and excited states. Nonzero displacements along high frequency vibrations result in faster wavepacket motion on the excited state potential energy surface and larger Raman intensities. The Raman intensity, I_{i-f}, for each frequency, ω_S, can be calculated using eq 1

$$I_{i-f} \propto \omega_I \omega_S^3 [\alpha_{fi}]^* [\alpha_{fi}] \quad (1)$$

with the scattering cross-section

$$[\alpha_{fi}] = \frac{i}{\hbar} \int_0^\infty \langle \phi_f | \phi(t) \rangle \times \exp\{i(\omega_k + \omega_I)t - i(E_{0-0} + \Gamma)t\}\, dt \quad (2)$$

where Γ is a phenomenological damping factor (cm^{-1}), E_{0-0} is the energy of the electronic origin transition (cm^{-1}), $\hbar\omega_k$ is the zero-point energy of mode (k), $\hbar\omega_I$ is energy of the incident excitation light (cm^{-1}), and $\langle \phi_f | \phi(t) \rangle$ is the time-dependent autocorrelation function. The latter can be calculated analytically from the following assumptions: (i) no change in force constants between ground and excited states, (ii) harmonic potential energy surfaces, (iii) no dependence of the transition moment on normal coordinates, (iv) no coupling between normal coordinates. Under these assumptions, the autocorrelation is described by eq 3

$$\langle \phi_f | \phi(t) \rangle = \prod_k \left\{ \exp\left[-\frac{\Delta_k^2}{2}(1 - \exp(-\omega_k t)) - \frac{i\omega_k t}{2} \right] \times (1 - \exp(-i\omega_k t))^{n_k} \times \frac{(-1)^{n_k} {\Delta_k}^{n_k}}{(2^{n_k} n_k!)^{1/2}} \right\} \quad (3)$$

where ω_k, n_k, and Δ_k represent the vibrational frequency (cm^{-1}), order (i.e., 0, 1, 2, ..., etc.) and displacement (dimensionless) of the k^{th} normal coordinate. Here, values of Δ_k are determined by adjusting this parameter for each mode until a good fit with experimental intensities is obtained.

Figure 6 shows a representative fit with an experimental Raman spectrum of encapsulated NFs. The calculation

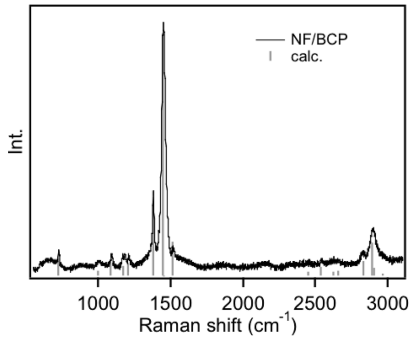

Figure 6. Experimental and calculated Raman spectrum of encapsulated P3HT NFs.

reproduces experimental intensities very well including the overtone and combination bands. Calculated values of Δ_k and their standard deviations are included in Table 1 along with Γ

Table 1. Frequencies ($\hbar\omega_k$) and Fitted Mode-Specific Vibrational Displacements (Δ_k) Used to Calculate Raman Spectra Including Overtone−Combination Bands[a]

P3HT NF/BCP		
mode (k)	$\hbar\omega_k$	Δ_k
ν_1	726	0.45
ν_2	996	0.19
ν_3	1087	0.27
ν_4	1170	0.21
ν_5	1207	0.23
ν_6	1378	0.50
ν_7	1448	0.78
ν_8	1513	0.27

[a] E_{0-0} = 15540 cm^{-1}; Γ = 400 cm^{-1}; ω_I = 20492 cm^{-1}.

and E_{0-0} values, which can be verified from optical lineshapes. Determination of multimode Δ_k values from resonance Raman intensity calculations now provides a more complete view of the excited state geometry changes in P3HT aggregates. For example, in calculations of P3HT aggregate optical lineshapes to extract exciton coupling strength it is typically assumed that the total Huang−Rhys factor ($S_k = 1/2\Delta_k^2$) is ~1.0 (a typical value observed in large oligothiophenes) and does not change significantly when the chains form π-stacked aggregates.[34] Furthermore, it is assumed that only the C=C mode is displaced (generally a good assumption) because this high frequency progression-forming mode usually dominates vibronic lineshapes. However, in delocalized electronic

dx.doi.org/10.1021/la3034337 | Langmuir 2012, 28, 16401−16407

structures such as aggregates, the amount of nuclear displacement should decrease due to sharing of electron density over a greater number of bonds. This is especially important for J-aggregates where increased delocalization along the individual chains implies the nuclear framework does not feel a change in electronic structure as much as in a localized system (i.e., oligomer or a single polymer chain). As shown in Table 1, estimates of Δ_k for the C=C mode are smaller than the typical reported value of ~1.4 which can be mostly explained by the inclusion of more displaced modes. In the typical single mode model analysis of aggregate optical spectra, linewidths must be arbitrarily increased to 'fill in' valleys between vibronic transitions. The validity of resonance Raman intensities to determine mode-specific Δ_k values can be appreciated from the relative time scales of PL and Raman processes. Namely, two-photon Raman transitions are virtually instantaneous thus producing a snapshot of the excited state geometry (Franck–Condon state) before the system relaxes into the emitting state geometry. Therefore, complementary optical and Raman spectroscopy measurements could, in principle, allow for accurate estimates of both exciton and vibronic coupling which has been impossible owing to substantial exciton coupling-induced line shape distortion effects. The only drawback to this approach is the possibility of overlapping states where interference can cause resonance de-enhancement effects, which would affect our Δ_k estimates. Because weakly resolved absorption spectrum corresponds to transitions from primarily aggregated P3HT chains, we assume interference effects are minor. Further exploration involving the generation and calculation of Raman excitation profiles is required to determine if the presence of close-lying excited states affect Δ_k values of the aggregate.

CONCLUSIONS

Encapsulation of P3HT NF J-aggregates by amphiphilic BCP molecules results in the formation of hierarchical superstructures, similar to previous work involving encapsulation of H-type NFs. J-aggregate behavior is mostly preserved although distortions in optical spectra make it difficult to quantify changes in exciton coupling. The primary evidence for this claim comes from single particle emission spectra of encapsulated NF superstructures that, in the absence of self-absorption effects, yield similar lineshapes as pristine J-type NFs. This is further supported by resonance Raman spectra of encapsulated BCP-NF structures which indicate no loss of the structural integrity of the NF (i.e., aggregation state). Overtone and combination band transitions appearing in resonance Raman spectra are observed, and analysis of intensities using the time-dependent theory of Raman spectroscopy permit estimations of vibrational mode-specific normal coordinate displacements, Δ_k. This result demonstrates that combinations of optical and Raman spectroscopic tools can be used to independently determine exciton and vibronic coupling terms of conjugated organic aggregates.

ASSOCIATED CONTENT

Supporting Information

TEM images of H- and J-type NFs; IR and off-resonance Raman spectra of NF samples; absorption, emission, and Raman spectra of pure BCP samples. This material is available free of charge via the Internet at http://pubs.acs.org.

AUTHOR INFORMATION

Corresponding Author

* E-mail: jkgrey@unm.edu.

Funding

Notes

The authors declare no competing financial interest.

ACKNOWLEDGMENTS

This work was supported by the National Science Foundation grant NSF-CHE 0955242 (J.K.G.).

REFERENCES

(1) Kim, Y.; Cook, S.; Tuladhar, S. M.; Choulis, S. A.; Nelson, J.; Durrant, J. R.; Bradley, D. D. C.; Giles, M.; McCulloch, I.; Ha, C.-S.; Ree, M. A Strong Regioregularity Effect in Self-organizing Conjugated Polymer Films and High-efficiency Polythiophene:fullerene Solar Cells. *Nat. Mater.* **2006**, *5*, 197–203.

(2) Xin, H.; Ren, G.; Kim, F. S.; Jenekhe, S. A. Bulk Heterojunction Solar Cells from Poly(3-butylthiophene)/Fullerene Blends: In Situ Self-Assembly of Nanowires, Morphology, Charge Transport, and Photovoltaic Properties. *Chem. Mater.* **2008**, *20*, 6199–6207.

(3) Koppe, M.; Brabec, C. J.; Heiml, S.; Schausberger, A.; Duffy, W.; Heeney, M.; McCulloch, I. Influence of Molecular Weight Distribution on the Gelation of P3HT and Its Impact on the Photovoltaic Performance. *Macromolecules* **2009**, *42*, 4661–4666.

(4) Gao, Y.; Martin, T. P.; Thomas, A. K.; Grey, J. K. Resonance Raman Spectroscopic- and Photocurrent Imaging of Polythiophene/Fullerene Solar Cells. *J. Phys. Chem. Lett.* **2010**, *1*, 178–182.

(5) Wang, X.; Zhang, D.; Braun, K.; Egelhaaf, H.-J.; Brabec, C. J.; Meixner, A. J. High-Resolution Spectroscopic Mapping of the Chemical Contrast from Nanometer Domains in P3HT:PCBM Organic Blend Films for Solar-Cell Applications. *Adv. Funct. Mater.* **2010**, *20*, 492–499.

(6) Brinkmann, M. Structure and Morphology Control in Thin Films of Regioregular Poly(3-hexylthiophene). *J. Polym. Sci., Part B* **2011**, *49*, 1218–1233.

(7) Sirringhaus, H.; Brown, P. J.; Friend, R. H.; Nielsen, M. M.; Bechgaard, K.; Langeveld-Voss, B. M. W.; Spiering, A. J. H.; Janssen, R. A. J.; Meijer, E. W.; Herwig, P.; de Leeuw, D. M. Two-Dimensional Charge Transport in Self-Organized, High-mobility Conjugated Polymers. *Nature* **1999**, *401*, 685–688.

(8) Yang, H.; Shin, T. J.; Yang, L.; Cho, K.; Ryu, C. Y.; Bao, Z. Effect of Mesoscale Crystalline Structure on the Field-Effect Mobility of Regioregular Poly(3-hexylthiophene) in Thin-Film Transistors. *Adv. Funct. Mater.* **2005**, *15*, 671–676.

(9) Diebel, C.; Dyakonov, V. Polymer–Fullerene Bulk Heterojunction Solar Cells. *Rep. Prog. Phys.* **2010**, *73*, 096401.

(10) Brown, P. J.; Sirringhaus, H.; Harrison, M.; Shkunov, M.; Friend, R. H. Optical Spectroscopy of Field-Induced Charge in Self-Organized High Mobility Poly(3-hexylthiophene). *Phys. Rev. B* **2001**, *63*, 125204.

(11) Singh, K. A.; Sauve, G.; Zhang, R.; Kowalewski, T.; McCullough, R. D.; Porter, L. M. Dependence of Field-Effect Mobility and Contact Resistance on Nanostructure in Regioregular Poly(3-hexylthiophene) Thin Film Transistors. *Appl. Phys. Lett.* **2008**, *92* (26), 263303/1–263303/3.

(12) Salim, T.; Sun, S.; Wong, L. H.; Xi, L.; Foo, Y. L.; Lam, Y. M. The Role of Poly(3-hexylthiophene) Nanofibers in an All-Polymer Blend with a Polyfluorene Copolymer for Solar Cell Applications. *J. Phys. Chem. C* **2010**, *114*, 9459–9468.

(13) Roehling, J. D.; Arslan, I.; Moule, A. J. Controlling Microstructure in Poly(3-hexylthiophene) Nanofibers. *J. Mater. Chem.* **2012**, *22*, 2498–2506.

(14) Lee, S. W.; Lee, H. J.; Choi, J. H.; Koh, W. G.; Myoung, J. M.; Hur, J. H.; Park, J. J.; Cho, J. H.; Jeong, U. Periodic Array of Polyelectrolyte-Gated Organic Transistors from Electrospun Poly(3-hexylthiophene) Nanofibers. *Nano Lett.* **2009**, *10*, 347–351.

(15) Chen, J.-Y.; Kuo, C.-C.; Lai, C.-S.; Chen, W.-C.; Chen, H.-L. Manipulation on the Morphology and Electrical Properties of Aligned Electrospun Nanofibers of Poly(3-hexylthiophene) for Field-Effect Transistor Applications. *Macromolecules* **2011**, *44*, 2883−2892.
(16) Berson, S.; De, B. R.; Bailly, S.; Guillerez, S. Poly(3-hexylthiophene) Fibers for Photovoltaic Applications. *Adv. Funct. Mater.* **2007**, *17*, 1377−1384.
(17) Spano, F. C. The Spectral Signatures of Frenkel Polarons in H- and J-Aggregates. *Acc. Chem. Res.* **2009**, *43*, 429−439.
(18) Spano, F. C.; Clark, J.; Silva, C.; Friend, R. H. Determining Exciton Coherence from the Photoluminescence Spectral Line Shape in Poly(3-hexylthiophene) Thin Films. *J. Chem. Phys.* **2009**, *130*, 074904/1−074904/16.
(19) Spano, F. C.; Yamagata, H. Vibronic Coupling in J-Aggregates and Beyond: A Direct Means of Determining the Exciton Coherence Length from the Photoluminescence Spectrum. *J. Phys. Chem. B* **2010**, *115*, 5133−5143.
(20) Yamagata, H.; Spano, F. C. Vibronic Coupling in Quantum Wires: Applications to Polydiacetylene. *J. Chem. Phys.* **2011**, *135*, 054906.
(21) Kanai, Y.; Grossman, J. C. Insights on Interfacial Charge Transfer Across P3HT/Fullerene Photovoltaic Heterojunction from Ab Initio Calculations. *Nano Lett.* **2007**, *7*, 1967−1972.
(22) Lan, Y.-K.; Huang, C.-I. Charge Mobility and Transport Behavior in the Ordered and Disordered States of the Regioregular Poly(3-hexylthiophene). *J. Phys. Chem. B* **2009**, *113*, 14555−14564.
(23) Sandstedt, C. A.; Rieke, R. D.; Eckhardt, C. J. Solid-State and Solvatochromic Spectra of a Highly Regular Polythiophene. *Chem. Mater.* **1995**, *7*, 1057−1059.
(24) Niles, E. T.; Roehling, J. D.; Yamagata, H.; Wise, A. J.; Spano, F. C.; Moulé, A. J.; Grey, J. K. J-Aggregate Behavior in Poly-3-hexylthiophene Nanofibers. *J. Phys. Chem. Lett.* **2012**, *3*, 259−263.
(25) Baghgar, M.; Labastide, J.; Bokel, F.; Dujovne, I.; McKenna, A.; Barnes, A. M.; Pentzer, E.; Emrick, T.; Hayward, R.; Barnes, M. D. Probing Inter- and Intrachain Exciton Coupling in Isolated Poly(3-hexylthiophene) Nanofibers: Effect of Solvation and Regioregularity. *J. Phys. Chem. Lett.* **2012**, *3*, 1674−1679.
(26) Kamps, A. C.; Fryd, M.; Park, S.-J. Hierarchical Self-Assembly of Aphoristic Semiconducting Polymers into Isolated, Bundled, and Branched Magnifiers. *ACS Nano* **2012**, *6*, 2844−2852.
(27) Samitsu, S.; Shimomura, T.; Heike, S.; Hashizume, T.; Ito, K. Effective Production of Poly(3-alkylthiophene) Nanofibers by means of Whisker Method using Anisole Solvent: Structural, Optical, and Electrical Properties. *Macromolecules* **2008**, *41* (21), 8000−8010.
(28) Gao, Y.; Grey, J. K. Resonance Chemical Imaging of Polythiophene/Fullerene Photovoltaic Thin Films: Mapping Morphology-Dependent Aggregated and Unaggregated C═C Species. *J. Am. Chem. Soc.* **2009**, *131*, 9654−9662.
(29) Roehling, J.; Moulé, A.; Arslan, I. Structure Study of Solution Formed Poly(3-hexylthiophene) Nanofibers. *Microsc. Microanal.* **2010**, *16*, 1362−1363.
(30) Ostrowski, D. P.; Lytwak, L. A.; Mejia, M. L.; Stevenson, K. J.; Holliday, B. J.; Vanden Bout, D. A. The Effects of Aggregation on Electronic and Optical Properties of Oligothiophene Particles. *ACS Nano* **2012**, *6*, 5507−5513.
(31) Heller, E. J. The Semiclassical Way to Molecular Spectroscopy. *Acc. Chem. Res.* **1981**, *14*, 368−375.
(32) Heller, E. J.; Sundberg, R.; Tannor, D. Simple Aspects of Raman Scattering. *J. Phys. Chem.* **1982**, *86*, 1822−1833.
(33) Shin, K. S. K.; Clark, R. J. H.; Zink, J. I. Calculation of Excited-State Geometries via the Time-Dependent theory of resonance Raman Spectroscopy: Application to the Complexes $Cs_4[W_2OCl_{10}]$ and $Cs_3[Re_2OCl_{10}]$. *J. Am. Chem. Soc.* **1990**, *112*, 3754−3759.
(34) Zhao, Z.; Spano, F. C. Multiple Mode Exciton-Phonon Coupling: Applications to Photoluminescence in Oligothiophene Thin Films. *J. Phys. Chem. C* **2007**, *111*, 6113−6123.